NICER data and a σ-field-dependent stiffness of the hadronic equation of state

E. E. Kolomeitsev [1,2] and D. N. Voskresensky [1,3]
[1]*Bogoliubov Laboratory of Theoretical Physics, Joint Institute for Nuclear Research, RU-141980 Dubna, Russia*
[2]*Department of Physics, Matej Bel University, SK-97401 Banska Bystrica, Slovakia*
[3]*National Research Nuclear University "MEPhI", Kashirskoe Avenue 31, RU-115409 Moscow, Russia*

(Received 17 April 2024; revised 25 June 2024; accepted 22 July 2024; published 6 August 2024)

Analyses for the NICER data indicate that there is no significant variation of compact star radii within the mass range of 1.4 to 2.0 solar masses. Yamamoto *et al.* [Phys. Rev. C **108**, 035811 (2023)] concluded recently that "this feature cannot be reproduced by the hadronic matter due to the softening of the equation of state (EoS) by hyperon mixing, suggesting the possible existence of quark phases in neutron-star interiors." Using a collection of 162 purely nucleonic, hyperonic, and quarkish EoSs from the CompOSE database and some other works, we verify that hyperons indeed lead to a significant difference in radii of stars of 1.4 and 2.0 solar masses, which diminishes in the presence of quarks. We compare the shapes of the mass-radius curves and show that hyperons and quarks in the neutron star cores prefer a particular curve shape with backbending. It is argued that the shape is controlled by the density dependence of the nuclear symmetry energy. We draw attention to the existence of a class of purely hadronic relativistic mean-field EoSs with scalar-field dependent hadron masses and coupling constants that satisfy the known constraints on the EoSs including the analyses of the new NICER data and the above requirement of insignificant variation of the neutron star radii.

DOI: 10.1103/PhysRevC.110.025801

I. INTRODUCTION

The advent of the multimessenger astronomy enables studies of neutron stars (NSs) through all the available tracers: cosmic rays, neutrinos, and electromagnetic and gravitational waves. New data provide more stringent constraints on the main NS parameters, which are used to get insight into hadron/nucleon interactions at suprasaturation densities [1]. Thanks to dedicated campaigns of radio pulsar timing measurements, several heavy NSs with masses greater than two solar masses were identified. The recently launched x-ray timing telescope, the Neutron Star Interior Composition Explorer (NICER), delivered several first joint measurements of star masses and radii. Based on the attempts to describe the new data, works have appeared with the conclusion that a purely hadronic equation of state (EoS) cannot fully account for them [2,3], and that a hybrid EoS involving subhadronic degrees of freedom (quarks, diquarks) is needed.

The purpose of this paper is, first, to restate which of the NS properties may appear problematic for the description with the purely hadronic EoSs, and, second, to point out a class of hadronic models that accommodate the new data.

II. MASSES OF NEUTRON STARS

For quite some time there has been a consensus that most NSs have masses near $1.4M_\odot$ [4], being produced in supernova explosions with masses close to the NS maximum mass $M_{\rm max} \simeq 1.5M_\odot$ [5]. Most of the existing hadronic EoSs could describe NSs with such masses. Also such a very narrow NS mass distribution offered a convenient way to explain the NS cooling data within the minimal cooling plus direct Urca (DU) scenario [6,7] without including in-medium effects. In contrast, a nuclear medium cooling scenario was developed in Refs. [8–11]. It relied on the assumption that NSs with measured surface temperatures (first data fixed only upper limits on surface temperatures) have very different masses and that NS neutrino emissivity depends strongly on the NS density, i.e. the NS mass, since the in-medium pion exchange significantly affects the two-nucleon reaction rates, whereas the DU reaction is not allowed [8,12]. This approach has been supported by the discovery of a light pulsar with mass $1.25M_\odot$ in the double pulsar system J0737−3039 [13] and by the growing evidence for the existence of NSs with masses greater than $1.5M_\odot$ [14]. It is now well established that NS masses vary over a wide interval [15]. The so-far lightest NS[1] with the well-measured mass of $1.174(4)M_\odot$ is the pulsar PSR J0453+1559 [16]. The masses of the heaviest pulsars are mainly derived from analyses of Shapiro delay measurements of pulsar binaries. The first well-measured masses were $1.908(16)M_\odot$ of PSR J1614−2230 [17–19] and $2.01(4)M_\odot$ for PSR J0348+0432 [20]. The current highest precisely measured mass is $2.08(7)M_\odot$ for PSR J0740+6620 [21,22]. Additional information is obtained from the photometry of binary systems of millisecond pulsars in tight <1 day orbits, with the companion heated and evaporated by the pulsar spindown power—the so-called spiders: black widows with substellar companions and redbacks with low-mass star companions. Among these objects there is the fastest rotating pulsar PSR J0952−0607 [23] whose mass is found to be $2.35(17)M_\odot$. A joint analysis including other spider pulsars

[1]A recent estimate for the CCO XMMU J173203.3−344518 mass, $0.77^{+0.20}_{-0.17}\,M_\odot$, reported in Ref. [52], will be discussed below.

in [24] leads to the conclusion that the minimum value for the maximum NS mass is $M_{\max} > 2.19M_\odot$ with 1σ confidence. It is to be noticed that all spider NSs are fast-rotating millisecond pulsars so one should include corrections for a possible increase of the star mass due to rotation, which is estimated in [25] as 3%. Therefore, the lower limit on the maximum NS mass should be lowered and, consequently, we would have $M_{\max} > 2.1M_\odot$. There is also a constraint on $M_{\max}$ from above. The authors of Ref. [26] combining gravitational wave observations of merging systems of binary NSs and quasiuniversal relations concluded that for a nonrotating NS the maximum mass should satisfy the constraint $M_{\max} < 2.33M_\odot$. If so, the value of $M_{\max}$ can be considered as a very-well-constrained quantity, $2.1M_\odot < M_{\max} < 2.33M_\odot$.

III. HYPERON AND Δ PUZZLES

Many purely nucleonic EoSs can satisfy the constraint $M_{\max} > 2.1M_\odot$; see Ref. [27] and the review of Skyrme models [28]. In the relativistic mean-field (RMF) modified Walecka models this inequality can be easily satisfied by choosing a sufficiently small effective nucleon mass at the saturation density as an input parameter; see Fig. 6 in Ref. [29]. However, allowing for the existence of strange particles in the model and the population of the corresponding Fermi seas, one realizes [30,31] that, by employing an empirically motivated two-body hyperon—nucleon potential, hyperons appear in NS matter already at baryon densities $\gtrsim (2\text{–}3)n_0$, where $n_0 \simeq 0.16$ fm^{-3} is the nuclear saturation density. The coupling constants of hyperons with vector mesons were interrelated by SU(6) symmetry relations; cf. [32]. As a result, the maximum masses of NSs with hyperons fall below not only $2M_\odot$ but also below $1.4M_\odot$. This was called in the literature the "hyperon puzzle,", which can be avoided by artificially preventing the appearance of hyperons or by including the hyperon-nucleon and/or hyperon-hyperon density-dependent repulsion, e.g., due to three-body forces [33]; see the discussion in Ref. [34]. In the framework of RMF models one can include the hyperon-hyperon repulsion mediated by a ϕ-meson mean field and/or use a different choice of hyperon-meson coupling constants beyond the quark counting within the SU(6) symmetry (see, e.g., Ref. [35]) to increase the NS mass. The similar "Δ puzzle" with the occupation of Δ isobar Fermi seas was identified in Ref. [36].

Another aspect of the hyperon puzzle is that the presence of hyperons in the NS interiors allows efficient DU reactions on hyperons (HDU), e.g., $\Lambda \to p + e + \bar{\nu}$, leading to very fast cooling of NSs with masses $M > M_{\rm HDU}$, where $M_{\rm HDU}$ is the NS mass at which the first hyperons appear in the star center. This second part of the problem is solved within the nuclear medium cooling scenario in [37,38].

IV. RADII OF NEUTRON STARS

In the early 2000s, experimental data on NS radii began to appear: from analyses of quasiperiodic oscillations in the low-mass x-ray binary system 4U 0614+09 [39], the thermal emission of the bright isolated NS RX J1856.5−3754 [40], thermonuclear x-ray bursts from NSs in low-mass x-ray binaries [41,42], and pulse-phase-resolved x-ray spectroscopy [43,44]. See also the Bayesian analysis of combined data in [45]. In most of these works, the masses of the studied objects were poorly constrained and only broad regions on the mass-radius plane (in some cases not even overlapping) were marked as allowed. This situation began to change with the launch of the NICER observatory. In its first measurement campaigns NICER studied the millisecond pulsar PSR J0030+0451, whose mass was found in two independent analyses to be $1.34^{+0.15}_{-0.16}M_\odot$ [46] and $1.44^{+0.15}_{-0.14}M_\odot$ [47] and the inferred radius was determined to be $12.71^{+1.14}_{-1.19}$ km in [46] and $13.02^{+1.24}_{-1.06}$ km in [47]. NICER then turned to one of the heaviest NSs, object PSR J0740+6620. The radius was found to be $13.7^{+2.6}_{-1.5}$ km in [48] and $12.39^{+1.30}_{-0.98}$ km in [49]. Applying the two-star radius measurements with the tidal deformability constraints to three different frameworks for EoS, Ref. [48] provided the following 68% credible intervals of the radius estimates:

$$R_{1.4M_\odot} = 12.45(65)\ \text{km}, \quad R_{2.0M_\odot} = 12.35(75)\ \text{km}. \tag{1}$$

The NICER data [46–49] have been incorporated, in Ref. [50], into the joint analysis of the NS EoS, using a nonparametric EoS model based on Gaussian processes and combining information from other x-ray, radio, and gravitational wave observations of NSs. The results are

$$R_{1.4M_\odot} = 12.56^{+1.00}_{-1.07}\ \text{km [47] and } 12.34^{+1.01}_{-1.25}\ \text{km [46]}, \tag{2}$$

$$R_{2.0M_\odot} = 12.41^{+1.00}_{-1.10}\ \text{km [48] and } 12.09^{+1.07}_{-1.17}\ \text{km [49]}. \tag{3}$$

These analyses show that, despite significant statistical uncertainties, the derived NS radii are consistent with being equal over a wide mass range, with a radius difference of

$$\Delta R_{(1.4\text{–}2.0)M_\odot} \equiv R_{1.4M_\odot} - R_{2.0M_\odot} = \begin{cases} 0.12^{+0.85}_{-0.83}\ \text{km} & (\text{Miller } et\ al.\ [47,48]), \\ 0.20^{+0.8}_{-0.82}\ \text{km} & (\text{Riley } et\ al.\ [46,49]); \end{cases} \tag{4}$$

see Table II in [50]. The results of the combined analyses collected in Table 4 in Ref. [48] assume that $-0.48 \lesssim \Delta R_{(1.4\text{–}2.0)M_\odot} \lesssim 0.35$ km. The lower limit $\Delta R_{(1.4\text{–}2.0)M_\odot} \simeq -0.68$ km follows from the direct NICER measurement by Miller *et al.* [47,48], while the results by Riley *et al.* [46,49] give the upper limit $\Delta R_{(1.4\text{–}2.0)M_\odot} \simeq 0.32$ km. Reference [51] investigated the additional effect on the EoS of the jointly estimated mass and radius of PSR J0740+6620 presented in [49] by analyzing a combined data set from x-ray telescopes NICER and XMM-Newton. They concluded that $R_{1.4M_\odot} \approx R_{1.8M_\odot} \approx R_{2.0M_\odot}$ within 1 km precision.

The lightest NS identified as the central compact object XMMU J173203.3−344518 could have a rather small radius $10.4^{+0.86}_{-0.78}$ km within 1σ confidence according to Ref. [52]. If confirmed, it would be an intriguing possibility of a superdense compact object different from a NS [53]. However, as pointed in Ref. [54], the results of Ref. [52] would change if the distance to the object is revised. The authors of Ref. [54] used the Gaia parallax measurements of the optical star and estimated the distance to the object to be shorter by a factor 1.28. Consequently, they obtained the larger mass of

$0.83^{+0.17}_{-0.13}\,M_\odot$ and the larger radius $11.25^{+0.53}_{-0.37}$ km for XMMU J173203.3−344518.

V. EoS AND EMPIRICAL CONSTRAINTS

Typical hadronic EoSs are challenged by the requirement of simultaneous fulfillment of empirical constraints gained in studies of various nuclear systems: atomic nuclei, heavy-ion collisions, and astrophysics. The most difficult task is to unite the description of the particle flow in heavy-ion collision requiring a soft EoS for the isospin-symmetric matter [55] and a large value of the maximum NS mass requiring a stiff EoS for the NS matter; see the discussion in Ref. [27]. To resolve this problem in the framework of RMF models, the baryon-density dependence of hadron coupling constants was suggested in Refs. [56,57]. In this case, the construction of thermodynamically consistent quantities requires additional care. In Ref. [29] we proposed the RMF model with scaling of hadron masses and coupling constants, the SHMC model, in which hadron masses and meson–baryon coupling constants are dependent on the σ mean field. For infinite nuclear matter, the scaling functions for masses and coupling constants enter the EoS only as a ratio, whose dependence on the σ field is chosen to gain the best description of empirical constraints that minimizes the number of fitted parameters. The σ-field scaling of RMF mass terms was motivated by experimental hints on the modification of hadronic masses and widths in hadronic matter and arguments for partial symmetry breaking with a baryon density increase. So, it looks natural that within the RMF approach not only baryon mass terms but also the mass terms of σ, ω, ρ, and ϕ meson fields should be similarly dependent on the σ field in the medium. In the SHMC models we deal with the usual Lagrangian approach, and the derivation of thermodynamic quantities follows without difficulty. The models KVR and KVOR of such a type, formulated in [29] and named so in [27], satisfied most of the constraints on the EoS known at that time from analysis of nuclei, heavy-ion collisions, and NSs, including the particle flow, DU, and maximum NS mass constraints; cf. Table V in Ref. [27]. To describe the new data on NS masses together with the flow constraint, two families of models (labeled MKVOR and KVORcut) were constructed in Refs. [58–60] based on the KVOR model. The models implement various versions of the stiffening mechanism (the cut mechanism) developed in [61], which aims at leveling off the sigma-field increase at some specified value. As a result, the effective baryon masses stop decreasing at some chosen value of the density $n_* \gtrsim (2\text{–}4)n_0$. Some microscopic support for such in-medium nucleon mass variation can be found in the renormalization group approach [62]. Also, if the decrease of the nucleon mass is determined by a decrease of the quark condensate in the medium, several mechanisms lead to a strong reduction of the condensate decrease rate at higher densities [63]. In the KVORcut family, the cut mechanism (strong variation of parameters with σ) is included in the ω-field sector, whereas in the MKVOR family the cut-mechanism is implemented in the ρ-meson sector. Therefore, we could push up the maximum NS mass and simultaneously satisfy the particle flow constraint from heavy-ion collisions since there is no ρ meson contribution for the isospin-symmetric matter.

The SHMC models were used in studies of heavy-ion collisions and NSs in Refs. [37,38,58–61,64–68], demonstrating that the maximum NS mass is $M_{\max} > (2\text{–}2.2)M_\odot$ even in the presence of hyperons and Δ baryons. Also, the models fulfill the constraints on the EoS of isospin symmetric matter from the nucleon flow and kaon production, giant monopole resonances, the constraints on the symmetry energy from neutron-proton elliptic flow difference measured by the FOPI-LAND experiment, and nuclear analog isobaric states. The MKVOR model was tuned to produce the EoS of purely neutron matter, which lies within the uncertainty region estimated within the chiral effective field theory in Ref. [69]. Comparison with the recent chiral calculations collected in Ref. [70] shows that also KVORcut03 model passes through the uncertainty region. The models describe appropriately optical nucleon potential $U(n)$, and for $n \lesssim n_0$ we appropriately recover the results of the chiral perturbation theory. In the case of the beta-equilibrium matter the DU constraint is fulfilled. The NS cooling data are also properly described even with hyperons taken into account [37,38]. The NS deformability calculated with our MKVOR-based models fits within the 90% confidence region obtained from the GW170817 gravitational wave signal. For the KVORcut03-based model, the results lie on a border of the 90% confidence region [71]. Thus, most of the presently known constraints are satisfied with the purely hadronic EoSs obtained with the SHMC model. For convenience of the reader, we briefly discuss specifics of the energy-density functional of the SHMC model in the Appendix. Further details can be found in [29,58–61,67].

Usually, new degrees of freedom appearing in a phase transition lead to a decrease of a thermodynamic potential that necessarily results in the EoS softening. Nevertheless, the maximum NS mass remains above the modern empirical constraints in our SHMC models [58–60] even in the presence of hyperons and Δ's. Reference [71] also demonstrated the possibility that in the SHMC models the most massive NSs may contain a hadron-quark pasta phase and quark cores, satisfying the maximum NS mass constraint. In Ref. [72] the hybrid star cooling scenario is shown to be compatible with the NS cooling data, provided the density dependence of diquark gaps is taken into account and the nuclear medium cooling scenario is used for the description of the hadronic part of the NSs.

Description of the outer part of the NS, the crust, which is important for the intermediate-mass stars ($\approx 1.4M_\odot$), is rather complicated because it requires a treatment of inhomogeneous matter. For the full thermodynamic consistency it would be necessary to describe the crust with a possible pasta phase and clusters transforming into neutron reach nuclei. Since models and, especially, methods used to derive the EoS for high baryon densities are often not suitable for the description of finite nuclei, the common practice is to attach an already established, phenomenologically constrained EoS for the crust to the core EoS. The SHMC models, which we consider, are matched with the BPS EoS [73], as described in detail in Appendix A in Ref. [59]. We followed logic similar

to that in Ref. [74]. Uncertainties of such a matching are discussed in Refs. [75,76]. In Ref. [77] it was argued that the thickness of the crust can be evaluated without having detailed knowledge of the EoS in this region, solution of the Tolman-Oppenheimer-Volkoff equation, and the condition that the baryon chemical potential is continuous in the crust, as it must be for fully catalyzed matter. Using Eq. (17) from the latter work, we obtain the crust thickness of the $1.4M_\odot$ NS, which differs from the calculations with our matched EoS by $\lesssim 100$ m. This gives an estimate for the uncertainty of our calculation of the radius $R_{1.4M_\odot}$. For heavier NS the crust is thinner and the uncertainty in $R_{2.0M_\odot}$ is expected to be still smaller.

To avoid the EoS softening in the phase transition constructed by matching of thermodynamical potential, the authors of Ref. [78] suggested the so-called "three-window scenario" assuming an enforced transition from the purely hadronic phase to a crossover phase at some density $n_{c1} \sim 2n_0$, which at density $n_{c2} \sim (4\text{–}7)n_0$ changes to quark matter. By this logic one can use the nuclear equation of state only at densities $n < n_{c1}$, some quark model at $n > n_{c2}$, and a smooth interpolation in between. Such a picture could be supported by the quark percolation conjecture [79,80] assuming that quarks may begin to "jump" between nucleons at n_{c1} and, then, the fraction of "shared" quarks increases with a density increase. If this were so, the hadron phase would change smoothly to the quarkish phase even though the latter one has a higher value of the thermodynamic potential (resulting in a stiffer EoS) than the hadronic one; see discussions in Refs. [2,81,82]. Within the three-window scenario the hyperon and Δ puzzles get an almost trivial solution: as soon as the quark percolation starts, the formation of new baryonic states and the corresponding Fermi seas is forbidden. It should be noticed, however, that there is currently no quantitative description of the intermediate density phase. Moreover, the density interval $(2\text{–}4)n_0$ is well covered by low-energy heavy-ion collision experiments, whose interpretation does not require the introduction of quark matter. Also, the NS masses obtained in ordinary RMF EoSs corresponding to central densities $(2\text{–}4)n_0$ are still low, $(0.7\text{–}1.5)M_\odot$. Thus, within this approach, questions remain about the fulfillment of other constraints such as the flow constraint (covering densities $\lesssim 4.5n_0$) and the DU constraint suggesting absence of the neutrino DU reactions in NSs with $M \lesssim (1.35\text{–}1.5)M_\odot$; cf. [27].

VI. APPLICATION OF NEW NICER DATA

Recently Ref. [3] proposed interpreting the NICER data in favor of approximate independence of the NS radii on the star mass in the interval of the NS masses between $1.4M_\odot$ and $2.0M_\odot$ and to use the relation

$$R_{1.4M_\odot} \approx R_{2.0r}, \tag{5}$$

as a possible novel constraint on the NS EoS supported by the analysis of [51]. A similar relation was discussed in Ref. [83]. From attempts to satisfy this constraint the authors of Ref. [3] concluded that it cannot be fulfilled with the purely hadronic EoSs softened by the admixture of hyperons,

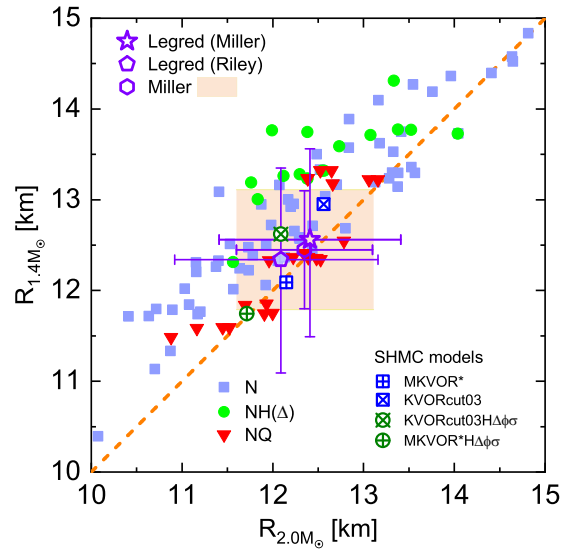

FIG. 1. Radii of NSs with masses 1.4 $M_\odot$ and $2.0M_\odot$ for the EoSs collected in Ref. [84]. Filled symbols stand for purely nucleonic EoSs (squares, N), EoSs with hyperons and/or Δ [circles, H(Δ)], and hybrid EoSs with nucleons and quarks (returned triangles, NQ). Symbols with error bars show the results by Legred *et al.* [50], Eqs. (2) and (3) using the NICER data [46,49] by Riley *et al.* (pentagon) and [47,48] by Miller *et al.* (star), and the results (1) of the combined analysis from [48] (hexagon). The error bars of the latter analysis are visualized by the colored rectangle. The dashed line represents the relation $R_{1.4M_\odot} = R_{2.0M_\odot}$. The EoSs for the SHMC models are depicted by open symbols: squares are for purely nucleonic models, MKVOR* (with the vertical cross) and KVORcut03 (with the diagonal cross); circles are for models with hyperons and Δ's, MKVORH*$\Delta\phi\sigma$ (with the vertical cross) and KVORcut03$\Delta\phi\sigma$ (with the diagonal cross).

indicating thereby in favor of the existence of quark or hybrid phases in NS interiors.

Before discussing the possibility of understanding new mass and radius measurements using SHMC models of purely hadronic EoS, including both hyperons and Δ's, we analyze typical EoSs for NSs used in the literature. We benefit from Ref. [84], where a set of cold NS EoSs was collected mainly from the CompOSE database [85] and from other works [86–88]. All together, 162 EoSs were selected in [84]. Dropping the EoSs with $M_{\max} < 2.0M_\odot$ we remain with 103 EoSs. In Fig. 1 we show the radii $R_{1.4M_\odot}$ and $R_{2.0M_\odot}$ calculated in the SHMC models and for the EoS collected in [84], among which there are 63 purely nucleonic EoSs (N), 18 EoSs with hyperons and/or Δ's [NH(Δ)], and 22 hybrid EoSs with nucleons and quarks (NQ) depicted by squares, circles and triangles, respectively. Symbols with error bars show the results of the analyses [50] [see Eq. (3)] and [48] [see Eq. (1)]. The colored rectangle visualizes the error bars given in (1). The dashed line stands for Eq. (5). We see that the radii for many purely nucleonic EoSs satisfy the constraint (5), i.e., the corresponding squares lie close to the dashed line. Also, many N-EoSs produce radii $R_{1.4(2.0)M_\odot}$ falling within the large experimental error bars. Open squares with crosses show two versions of the purely nucleonic SHMC models. The minimal

modification of the MKVOR model labeled MKVOR* in [60] prevents the effective nucleon mass from vanishing at any density. The MKVOR* square is closer to the dashed line than that for KVORcut03; cf. [59]. In case of the MKVOR* model the radius difference $\Delta R_{(1.4\text{–}2.0)M_\odot}$ is negative, -0.1 km, while for the KVORcut03 model it is positive, $+0.4$ km. We stress that these two models differ in the density dependence of the symmetry energy, which is weaker in the first model for $n > n_0$.

The inclusion of hyperons (or/and Δs) shifts the radii (circles) in Fig. 1 up from the dashed line. For those H(Δ) EoSs whose radii agree with Legred's analyses, the radius difference $\Delta R_{(1.4\text{–}2.0)M_\odot} \gtrsim 1$ km, and only one H(Δ) EoS is within error bars of the constraint (1), i.e., enters the colored rectangle. One more point satisfies this constraint marginally. Thus, indeed, among the EoSs collected in [84], the inclusion of hyperons complicates the fulfillment of the condition (5). In contrast, many NQ EoSs satisfy well this condition, and many triangles lie close to the dashed line. So, in favor of the statement [3] it is tempting to conclude that the quark admixture in the NS matter is necessary to reach the agreement with condition (5). However, the purely hadronic SHMC models with hyperons can also satisfy condition (5). Open circles with crosses in Fig. 1 show the radii for the models MKVOR*H$\Delta\phi\sigma$ and KVORcut03H$\Delta\phi\sigma$ [59,60]. The suffix "ϕ" means that in these models we included the ϕ-meson mean field providing repulsion among hyperons and took into account the scaling of the mean-field ϕ meson mass term similar to the scaling of other mean-field mass terms and the nucleon mass. As shown in Ref. [58] this scaling enhances the hyperon-hyperon repulsion and allows the solution of the hyperon puzzle. The suffix "σ" indicates that we include the effect of reducing hyperon-sigma coupling with a σ field increase, as follows, e.g., from the quark-meson coupling model [89]. We see that the KVORcut03H$\Delta\phi\sigma$ point enters the colored rectangle in Fig. 1, and MKVOR*H$\Delta\phi\sigma$ marginally satisfies this constraint. For the MKVOR*H$\Delta\phi\sigma$ model we have $\Delta R_{(1.4\text{–}2.0)M_\odot} = -0.03$ km and for KVORcut03H$\Delta\phi\sigma$ model 0.5 km.

The shape of the mass-radius curve can be characterized by the sign and magnitude of the derivative $R'(M)$ at the inflection point of the $R(M)$ curve, i.e., the point where $R''(M_{\rm infl}) = 0$. In Fig. 2 we illustrate the correlation between $\Delta R_{(1.4\text{–}2.0)M_\odot}$ and $R'(M_{\rm infl})$ for different types of the EoSs. If $R'(M_{\rm infl}) < 0$, then $M(R)$ is a monotonically decreasing function, shown in the left inset plot in Fig. 2. If $R'(M_{\rm infl}) > 0$, then $M(R)$ curve is nonmonotonic with a backbending, as shown in the right inset. We see that most of the NH(Δ) and NQ EoSs give the $M(R)$ curve with backbending, while the nucleonic (N) EoSs can produce the $M(R)$ curves with and without backbending. For MKVOR* and MKVOR*H$\Delta\phi\sigma$ EoSs, $R(M)$ curves have backbending and $R'(M_{\rm infl}) > 0$. These models are characterized by a softer density dependence of the symmetry energy than the KVORcut models. Respectively, the coefficient L characterizing the density dependence of the symmetry energy nearby $n \simeq n_0$ is smaller ($L \simeq 41$ MeV) for MKVOR-type models than that ($L \simeq 71$ MeV) for KVOR-type models. The model KVORcut03H$\Delta\phi\sigma$ demonstrates $R'(M_{\rm infl}) < 0$. The KVORcut03 EoS shows a tiny negative value of $R'(M_{\rm infl})$. The

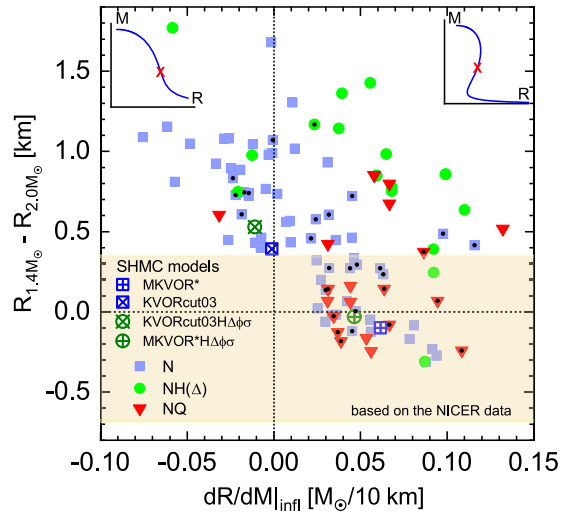

FIG. 2. Correlation between $\Delta R_{(1.4\text{–}2.0)M_\odot}$ and the form of the mass-radius curve characterized by the sign of the derivative $R'(M)$ at the inflection point (shown by crosses in the insertion plots as an illustration) for the same set of EoSs as in Fig. 1. All symbols have the same meaning as in Fig. 1. The color band indicates the interval $-0.68 < \Delta R_{(1.4\text{–}2.0)M_\odot} < 0.35$ km encompassing the results of different analyses; see Eq. (4) and the text below it. Central dots indicate the EoSs, which fall within the colored rectangle in Fig. 1 satisfying the radius constraint from the combined analysis of Ref. [48].

correlation between the density dependence of the symmetry energy and the shape of $M(R)$ curve is also visible in Fig. 1 of work [90] and in Fig. 5 of work [91] for the EoSs studied there. Existing NICER data are still not sufficient to determine if the $M(R)$ curve has the backbending. However there is a hope that the third generation of gravitational wave detectors [92] will permit measurement of the NS radius with an uncertainty of the order of 100m. If so, presence or absence of the backbending will be checked experimentally with a good accuracy.

The colored band in Fig. 2 indicates an interval of $-0.68 < \Delta R_{(1.4\text{–}2.0)M_\odot} < 0.35$ km motivated by the analyses [47,48]. Using central dots we additionally mark those EoSs whose NS radii occur within the colored rectangle in Fig. 1. Only these EoSs agree with empirical data (1) from the analysis [48]. None of the NH(Δ) EoSs can be found simultaneously in the colored rectangles in Figs. 1 and 2. The SHMC EoSs MKVOR* and MKVOR*H$\Delta\phi\sigma$ satisfy both constraints. The model KVORcut03 satisfies the constraint marginally. The model KVORcut03H$\Delta\phi\sigma$ does not fulfill it.

Finally, let us compare the NS mass-radius relations for the considered SHMC models with the available empirical constraints; see Fig. 3. All four models have $M_{\rm max} > 2.0M_\odot$. The NS mass constraint from the black widow pulsar J0952−0607 ($M_{\rm max} > 2.2M_\odot$) is satisfied by the purely nucleonic MKVOR* model and also by the MKVOR*H$\Delta\phi\sigma$ model with hyperons and Δ's. Accounting for the rotation correction [25], the lower edge of the constraint can be reduced to $2.1M_\odot$, then also the KVORcut03 EoS and marginally the KVORcut03H$\Delta\phi\sigma$ EoS will satisfy it. We stress that the mass-radius curves for all four SHMC EoSs go through

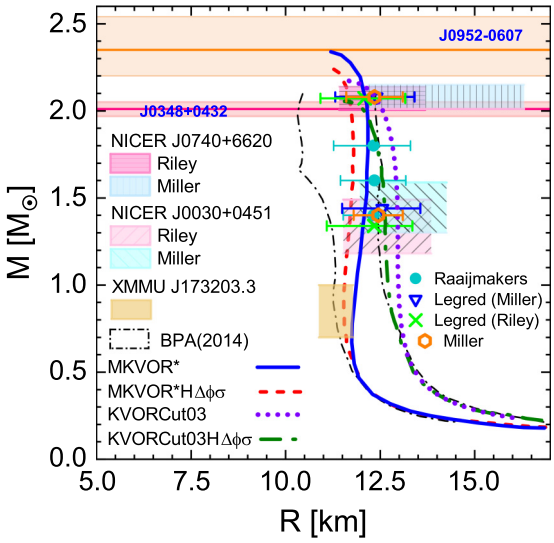

FIG. 3. The mass-radius relation for a cold nonrotating NS. Solid, dashed, dash-dotted and dotted lines show the result for four SHMC models discussed in text. Hatched regions show the results of NICER obtained by Miller *et al.* in [47,48] and Riley *et al.* in [46,49], and the XMMU data after the distance correction in Ref. [54]. The dash-dotted contour shows the M-R range from the Bayesian probability analysis (BPAs) [45]. Filled circles show the results of the analysis by Raaijmakers *et al.* [51]. The results of the combined analysis of Legred *et al.* [50] using data of Miller *et al.* and Riley *et al.* are shown by triangle and cross symbols, respectively. Hexagons represent the analysis of the data done in Ref. [48].

the results of extended analyses of the NICER data [50,51] including additional empirical and theoretical information. As for the results of the direct NICER measurements, the SHMC EoSs do not pass through the radius range obtained by Miller *et al.* [48] for the $2.0M_\odot$ NS; however, all agree with the range deduced by Riley *et al.* [49]. For the direct measurements presented in Refs. [46,47], the MKVOR*HΔ$\phi\sigma$ model does not pass through the 1σ range suggested for $R_{1.4M_\odot}$ in Ref. [47], but agrees with the result [46] and almost touches the 1σ error bar (hexagon in Fig. 3) given in the analysis of [48]; see Eq. (1). We note also that the reanalysis in Ref. [48], Eq. (1), reduces the tension between the direct NICER results by Miller *et al.* [47], $R_{1.4M_\odot} = 13.02^{+1.24}_{-1.06}$ km, and the constraint put on $R_{1.4M_\odot}$ in Ref. [93], where the authors used the chiral effective field theory and the gravitational wave observations of the binary NS merger GW170817. They claim $R_{1.4M_\odot} = 11.0^{+0.9}_{-0.6}$ km with 90% confidence. The XMMU rectangle shows the constraint obtained after the distance correction in Ref. [54]. The MKVOR-based models satisfy this constraint, unlike the KVORcut-based models. This difference may be related to the weaker density dependence of the symmetry energy in the former ones. In Fig. 3 we also see that stars with hyperons and Δ's have smaller radii than stars without.

VII. CONCLUSION

Using a set of 103 EoSs collected in Ref. [84] from the CompOSE database [85] and from Refs. [86–88], among which there are 18 EoSs with hyperons and/or Δ's and 22 hybrid NQ EoSs, we demonstrated that indeed most of the used hadronic EoSs with hyperons and/or Δ's [NH(Δ)] do not satisfy the condition conjectured in [3] that the stellar radius weakly changes with the mass increase from $1.4M_\odot$ to $2.0M_\odot$; see Eq. (5). According to the analyses of a combined data set from the x-ray telescopes NICER and XMM-Newton supplemented by the gravitational wave constraints and theoretical constraints on the EoSs [48,50,51] discussed above, the radius difference is limited to $-0.68 < \Delta R_{(1.4\text{–}2.0)M_\odot} < 0.35$ km. None of the NH(Δ) EoSs from the EoS collection in [84] satisfy both this constraint and the constraint (1) on stellar radii obtained in the analysis [48]. In contrast, the hybrid EoSs with nucleons and quarks constructed within the three-window scenario fulfill these constraints; see Fig. 1.

We analyzed the shape of the mass-radius curve, $M(R)$, for different EoSs and demonstrated that for the NH(Δ) and NQ EoSs it has, as a rule, backbending, as shown in Fig. 2. We also argued that this shape favors a smoother density dependence of the nuclear symmetry energy and a smaller value of L.

We showed that the hadronic relativistic mean-field models with the σ-field-scaled hadron masses and coupling constants (SHMC)—the KVORcut03- and MKVOR-based models—constructed in Refs. [58–60] pass most of the currently known constraints from experiments with nuclei, heavy-ion collisions, and compact stars, including the analyses of the new NICER mass-radius measurements. The MKVOR-type models with and without hyperons and Δ's satisfy well the condition (5) conjectured in [3]. The KVORcut03 EoS satisfies it marginally. The mass-radius curves for the considered SHMC models shown in Fig. 3 agree very well with the constraints based on the new NICER data.

A weak variation of the NS radius of the star mass for $M > 0.5M_\odot$ has been noticed already in works [58–60] and it is now supported by the NICER data and suggested as a constraint in Ref. [3]. We hope that our results can be treated in favor of RMF models including σ scaling not only of baryon masses but also of meson masses.

The presented analysis shows that the new NICER-data-based constraints on the NS radii are very selective to the EoS used in the NS descriptions. The future next-generation gravitational-wave observatory [92], Cosmic Explorer, is planned to detect NS mergers with a high rate that will enable the determination of stellar radii with a very high precision of 100 meters. Thus, the conjecture of Ref. [3] supported by our results [58–60] obtained with purely hadronic SHMC models and other results illustrated in Figs. 1–3 could be, hopefully, verified experimentally.

ACKNOWLEDGMENTS

We are grateful to Dmitri Ofengeim for discussing and sharing with us his collection of EoSs and mass-radius curves from Ref. [84]. The analysis of hadronic EoSs is carried out within the framework of the Russian Science Foundation program under Grant No. RSF 21-12-00061. The work is also partially supported by VEGA Grant No. 1/0521/22.

APPENDIX: THE ENERGY-DENSITY FUNCTIONAL OF SHMC MODELS

In this Appendix we briefly discuss the SHMC model constructed in Refs. [29,58–61,67]. The model is a generalization of the non-linear RMF model. Our model uses the effective coupling constants $g^*_{mb} = g_{mb}\chi_{mb}(\sigma)$ and hadron masses $m^*_i = m_i\Phi_i(\sigma)$, which are functions of the σ field, where index $m = \{\sigma, \omega, \rho, \phi\}$ lists the included mesonic fields, $b = (N, H, \Delta)$ indicates a baryon (nucleon $N = p, n$; hyperon $H = \Lambda, \Sigma, \Xi$; and Δ isobar). Index $i = (b, m)$ stands for a hadronic state, in general. Quantities $\chi_{mb}(\sigma)$ and $\Phi_i(\sigma)$ are some scaling functions.

After minimization with respect to the ω, $\vec{\rho}$, and ϕ mean fields the energy of the hadronic subsystem becomes, cf. Eqs. (1)–(8) in [60],

$$E[\{n_b\}, f] = \sum_b E_{\rm kin}(p_{{\rm F},b}, m_b\Phi_b(f)) + \frac{m_N^4 f^2}{2C_\sigma^2}\eta_\sigma(f) + \frac{1}{2m_N^2}\left[\frac{C_\omega^2 n^2}{\eta_\omega(f)} + \frac{C_\rho^2 n_I^2}{\eta_\rho(f)} + \frac{C_\phi^2 n_S^2}{\eta_\phi(f)}\right]. \quad \text{(A1)}$$

Here $C_M^2 = g_{MN}^2 m_N^2/m_M^2$ are dimensionless coupling constants of nucleons, N, interacting with the $M = \{\sigma, \omega, \rho\}$ meson mean fields, and $C_\phi^2 = g_{\omega N}^2 m_N^2/m_\phi^2$. The baryon, n, isospin vector, n_I, and strangeness, n_S, densities are defined as

$$n = \sum_b x_{\omega b} n_b, \quad n_I = \sum_b x_{\rho b} t_{3b} n_b,$$
$$n_S = \sum_H x_{\phi H} s_H n_H, \quad \text{(A2)}$$

$x_{mb} = g_{mb}/g_{mN}$ are the coupling constant ratios, t_{3b} is the isospin projection of baryon b, and s_H is its strangeness. The Fermi momentum of the baryon is related to the baryon density as $p_{{\rm F},b} = [6\pi^2 n_b/(2s_b + 1)]^{1/3}$, where s_b is the baryon spin. The baryon kinetic energy density is

$$E_{\rm kin}(p_{\rm F}, m, s) = (2s + 1)\int_0^{p_{\rm F}} \frac{p^2 dp}{2\pi^2}\sqrt{p^2 + m^2}.$$

The coupling constants of hyperons and Δ isobars to vector mesons in our approach are related to those of nucleons with the help of the SU(6) symmetry relations. The scalar meson coupling constants are constrained by hyperon and Δ potentials, $U_{H(\Delta)}(n_0)$, in the isospin symmetric nucleon matter at saturation. For hyperons these parameters are deduced from extrapolations of hyper-nucleus data and for Δ from calculations and pion photoproduction data; see Sec. 2.3 in [60].

The scaling function $\eta_\sigma(f)$ can be expressed in terms of the self-interaction potential $U(\sigma)$ as in the modified Walecka model. Putting $\eta_\omega = \eta_\rho = \eta_\phi = 1$, we would recover the standard nonlinear σ-ω model in the nonstrange sector. The functions $\eta_m(f) = \Phi_m^2/\chi_{mb}^2$ for $m = \omega, \rho, \phi$ are the ratios of scaling functions of vector-meson masses to the scaling function of hadron-nucleon coupling constants. We construct them to get the best agreement of the resulting EoS with empirical constraints. Following the concept of universality we tried first small variations of the scaling function $\eta_{\sigma,\omega} = 1 \pm 0.3$ (KVOR model), and took the scaling function η_ρ to ensure the steady increase of the f field with a density increase and to suppress the symmetry energy removing thereby the threshold for direct Urca reaction to larger densities [29]. Later, in Ref. [59] we implemented the cut mechanism [61] in the η_ω function (KVORcut models) or in the η_ρ function (MKVOR model) and additionally in the η_ω function (MKVOR* model). The parametrizations of the functions $\eta_{\sigma,\omega,\rho}$ for the considered models can be found in Appendices B of Refs. [60,67]. For the KVORcut03 and MKVOR* models used in this work the functions $\eta_{\sigma,\omega,\rho}(f)$ are shown in Fig. 1 in Refs. [60,67].

In the strange sector we add the ϕ meson field responsible for hyperon repulsion [35]. The coupling constant for the ϕ meson is unscaled, which results in the ϕ scaling function $\eta_\phi = (1 - f)^2$.

Various suffixes in the model labels denote the inclusion of hyperons (suffix H) and Δ isobars (suffix Δ) and the particular choice of scaling functions in the strangeness sector (ϕ).

For baryons we use the scaling function $\Phi_b(f) = 1 - x_{\sigma b}\xi_{\sigma b}\frac{m_N}{m_b}f$, where $\xi_{\sigma b}(f) = \chi_{\sigma b}/\chi_{\sigma N}$. Following [29] a universal scaling was used for nucleon and meson masses, $\Phi_m(f) \approx \Phi_N(f)$. The universality assumes that $\xi_{\sigma b} \simeq 1$. Such a behavior is motivated by ideas of the partial chiral symmetry breaking with increasing density. However, in the strange-sector we tried also a nonuniversal behavior of coupling constant following the results of the quark-meson coupling model [89], where the $\Lambda\sigma$ coupling decreases with the density. For the models labeled by the suffix (σ) we employed that $\xi_{\sigma b} \simeq 1$ for $n \lesssim n_0$ and decreases for higher densities reaching zero for densities when hyperons appear in the NS matter $n > n_{cH}$. Then, for calculations of the NS structure, there is no need to specify explicitly the dependence $\chi_{\sigma H}$ on f, as we may just use vacuum masses of the hyperon H. In this work we demonstrate results for the $H\Delta\phi\sigma$ models, since in these models the NS maximum mass proved to be a bit higher than for the $H\Delta\phi$ models.

The coefficients $C_{\sigma,\omega,\rho}$ are adjusted to reproduce the saturation properties: density $n_0 = 0.16$ fm^{-3}, the binding energy $\varepsilon_0 = -16$ MeV, and the effective nucleon mass chosen as $m_N^*(n_0) = 0.805\, m_N$ for the KVORcut03-based model and 0.730 for the MKVOR-based models. Parameters of the expansion of the nucleon binding energy per nucleon near the nuclear saturation density n_0,

$$\mathcal{E} = \varepsilon_0 + \frac{K}{2}\epsilon^2 - \frac{K'}{6}\epsilon^3 + \cdots + \beta^2\left(J + L\epsilon + \frac{K_{\rm sym}}{2}\epsilon^2 + \cdots\right) + \cdots, \quad \text{(A3)}$$

$\epsilon = (n - n_0)/3n_0$ and $\beta = (n_n - n_p)/n$, which we use in our KVORcut03 and MKVOR based models are presented in Table I.

TABLE I. The properties of the isospin symmetric matter at saturation for KVORcut03 and MKVOR models (in MeV).

EoS	K	J	L	K'	$K_{\rm sym}$
KVORcut03	275	32	71	422	−86
MKVOR	240	30	41	557	−158

[1] J. Lattimer, Neutron stars and the nuclear matter equation of state, Annu. Rev. Nucl. Part. Sci. **71**, 433 (2021).

[2] G. Baym, T. Hatsuda, T. Kojo, P. D. Powell, Y. Song, and T. Takatsuka, From hadrons to quarks in neutron stars: a review, Rep. Prog. Phys. **81**, 056902 (2018).

[3] Y. Yamamoto, N. Yasutake, and T. A. Rijken, Quark phases in neutron stars consistent with implications from NICER observations, Phys. Rev. C **108**, 035811 (2023).

[4] S. E. Thorsett and D. Chakrabarty, Neutron star mass measurements. I. Radio pulsars, Astrophys. J. **512**, 288 (1999).

[5] G. E. Brown and H. A. Bethe, A scenario for a large number of low-mass black holes in the galaxy, Astrophys. J. **423**, 659 (1994).

[6] D. Page, J. M. Lattimer, M. Prakash, and A. W. Steiner, Minimal cooling of neutron stars: A new paradigm, Astrophys. J. Suppl. Ser. **155**, 623 (2004).

[7] D. G. Yakovlev, O. Y. Gnedin, A. D. Kaminker, K. P. Levenfish, and A. Y. Potekhin, Neutron star cooling: theoretical aspects and observational constraints, Adv. Space Res. **33**, 523 (2004).

[8] D. N. Voskresensky and A. V. Senatorov, Emission of neutrinos by neutron stars, ZhETF **90**, 1505 (1986) [Sov. Phys. JETP **63**, 885 (1986)].

[9] C. Schaab, D. Voskresensky, A. D. Sedrakian, F. Weber, and M. K. Weigel, Impact of medium effects on the cooling of nonsuperfluid and superfluid neutron stars, Astron. Astrophys. **321**, 591 (1997).

[10] D. N. Voskresensky, Neutrino cooling of neutron stars: Medium effects, *Physics of Neutron Star Interiors*, Lecture Notes in Physics Vol. 578 (Springer, Berlin, 2001), p. 467.

[11] D. Blaschke, H. Grigorian, and D. N. Voskresensky, Cooling of neutron stars: Hadronic model, Astron. Astrophys. **424**, 979 (2004).

[12] D. N. Voskresensky and A. V. Senatorov, Pion excitations in a nucleonic medium may be pertinent to the luminosity of neutron stars, JETP Lett. **40**, 1212 (1984).

[13] A. G. Lyne, M. Burgay, M. Kramer, A. Possenti, R. Manchester, F. Camilo, M. A. McLaughlin, D. R. Lorimer, N. D'Amico, B. C. Joshi, J. Reynolds, and P. C. C. Freire, A double-pulsar system: A rare laboratory for relativistic gravity and plasma physics, Science **303**, 1153 (2004).

[14] D. J. Nice, E. M. Splaver, I. H. Stairs, O. Löhmer, A. Jessner, M. Kramer, and J. M. Cordes, A 2.1 $M_\odot$ pulsar measured by relativistic orbital decay, Astrophys. J. **634**, 1242 (2005).

[15] J. M. Lattimer, The nuclear equation of state and neutron star masses, Annu. Rev. Nucl. Part. Sci. **62**, 485 (2012).

[16] J. G. Martinez, K. Stovall, P. C. C. Freire, J. S. Deneva, F. A. Jenet, M. A. McLaughlin, M. Bagchi, S. D. Bates, and A. Ridolfi, Pulsar J0453+1559: A double neutron star system with a large mass asymmetry, Astrophys. J. **812**, 143 (2015).

[17] P. B. Demorest, T. Pennucci, S. M. Ransom, M. S. E. Roberts, and J. W. T. Hessels, A two-solar-mass neutron star measured using Shapiro delay, Nature (London) **467**, 1081 (2010).

[18] E. Fonseca *et al.*, The NANOgrav nine-year data set: mass and geometric measurements of binary millisecond pulsars, Astrophys. J. **832**, 167 (2016).

[19] Z. Arzoumanian *et al.*, The NANOGrav 11-year data set: High-precision timing of 45 millisecond pulsars, Astrophys. J. Suppl. Series **235**, 37 (2018).

[20] J. Antoniadis *et al.*, A massive pulsar in a compact relativistic binary, Science **340**, 1233232 (2013).

[21] H. T. Cromartie *et al.* (NANOGrav Collaboration), Relativistic shapiro delay measurements of an extremely massive millisecond pulsar, Nat. Astron. **4**, 72 (2019).

[22] E. Fonseca *et al.*, Refined mass and geometric measurements of the high-mass PSR J0740+6620, Astrophys. J. Lett. **915**, L12 (2021).

[23] R. W. Romani, D. Kandel, A. V. Filippenko, T. G. Brink, and W. Zheng, PSR J0952-0607: The fastest and heaviest known galactic neutron star, Astrophys. J. Lett. **934**, L17 (2022).

[24] D. Kandel and R. W. Romani, An optical study of the black widow population, Astrophys. J. **942**, 6 (2023).

[25] L. Brandes, W. Weise, and N. Kaiser, Evidence against a strong first-order phase transition in neutron star cores: Impact of new data, Phys. Rev. D **108**, 094014 (2023).

[26] L. Rezzolla, E. R. Most, and L. R. Weih, Using gravitational-wave observations and quasi-universal relations to constrain the maximum mass of neutron stars, Astrophys. J. Lett. **852**, L25 (2018).

[27] T. Klähn, D. Blaschke, S. Typel, E. N. E. van Dalen, A. Faessler, C. Fuchs, T. Gaitanos, H. Grigorian, A. Ho, E. E. Kolomeitsev, M. C. Miller, G. Röpke, J. Trümper, D. N. Voskresensky, F. Weber, and H. H. Wolter, Constraints on the high-density nuclear equation of state from the phenomenology of compact stars and heavy-ion collisions, Phys. Rev. C **74**, 035802 (2006).

[28] J. R. Stone, J. C. Miller, R. Koncewicz, P. D. Stevenson, and M. R. Strayer, Nuclear matter and neutron-star properties calculated with the Skyrme interaction, Phys. Rev. C **68**, 034324 (2003).

[29] E. E. Kolomeitsev and D. N. Voskresensky, Relativistic mean-field models with effective hadron masses and coupling constants, and ρ-condensation, Nucl. Phys. A **759**, 373 (2005).

[30] J. Schaffner-Bielich, Hypernuclear physics for neutron stars, Nucl. Phys. A **804**, 309 (2008).

[31] H. Đapo, B.-J. Schaefer, and J. Wambach, Appearance of hyperons in neutron stars, Phys. Rev. C **81**, 035803 (2010).

[32] E. N. E. van Dalen, G. Colucci, and A. Sedrakian, Constraining hypernuclear density functional with Λ-hypernuclei and compact stars, Phys. Lett. B **734**, 383 (2014).

[33] S. Petschauer, J. Haidenbauer, N. Kaiser, U.-G. Meißner, and W. Weise, Hyperon-nuclear interactions from SU(3) chiral effective field theory, Front. Phys. **8**, 12 (2020).

[34] W. Weise, Sound velocity, equation of state and strangeness in neutron star matter, EPJ Web Conf. **291**, 01007 (2024).

[35] S. Weissenborn, D. Chatterjee, and J. Schaffner-Bielich, Hyperons and massive neutron stars: vector repulsion and SU(3) symmetry, Phys. Rev. C **85**, 065802 (2012); **90**, 019904(E) (2014).

[36] A. Drago, A. Lavagno, G. Pagliara, and D. Pigato, Early appearance of Δ isobars in neutron stars, Phys. Rev. C **90**, 065809 (2014).

[37] H. Grigorian, E. E. Kolomeitsev, K. A. Maslov, and D. N. Voskresensky, On cooling of neutron stars with a stiff equation of state including hyperons, Universe **4**, 29 (2018).

[38] H. Grigorian, D. N. Voskresensky, and K. A. Maslov, Cooling of neutron stars in "nuclear medium cooling scenario" with stiff equation of state including hyperons, Nucl. Phys. A **980**, 105 (2018).

[39] S. van Straaten, E. C. Ford, M. van der Klis, M. Méndez, and P. Kaaret, Relations between timing features and colors in the x-ray binary 4U 0614+09, Astrophys. J. **540**, 1049 (2000).

[40] J. Trümper, V. Burwitz, F. Haberl, and V. Zavlin, The puzzles of RX J1856.5-3754: neutron star or quark star? Nucl. Phys. B **132**, 560 (2004).

[41] F. Özel, D. Psaltis, T. Güver, G. Baym, C. Heinke, and S. Guillot, The dense matter equation of state from neutron star radius and mass measurements, Astrophys. J. **820**, 28 (2016).

[42] V. F. Suleimanov, J. Poutanen, J. Nättilä, J. J. E. Kajava, M. G. Revnivtsev, and K. Werner, The direct cooling tail method for X-ray burst analysis to constrain neutron star masses and radii, Mon. Not. R. Astron. Soc. **466**, 906 (2017).

[43] S. Bogdanov, The nearest millisecond pulsar revisited with XMM-Newton: improved mass–radius constraints for PSR J0437-4715, Astrophys. J. **762**, 96 (2013).

[44] V. Hambaryan, R. Neuhäuser, V. Suleimanov, and K. Werner, Observational constraints of the compactness of isolated neutron stars, J. Phys.: Conf. Ser. **496**, 012015 (2014).

[45] J. M. Lattimer and A. W. Steiner, Neutron star masses and radii from quiescent low-mass X-ray binaries, Astrophys. J. **784**, 123 (2014).

[46] T. E. Riley *et al.*, A NICER view of PSR J0030+0451: Millisecond pulsar parameter estimation, Astrophys. J. Lett. **887**, L21 (2019).

[47] M. C. Miller *et al.*, PSR J0030+0451 mass and radius from NICER data and implications for the properties of neutron star matter, Astrophys. J. Lett. **887**, L24 (2019).

[48] M. C. Miller *et al.*, The radius of PSR J0740+6620 from NICER and XMM-Newton data, Astrophys. J. Lett. **918**, L28 (2021).

[49] T. E. Riley *et al.*, A NICER view of the massive pulsar PSR J0740+6620 informed by radio timing and XMM-Newton spectroscopy, Astrophys. J. Lett. **918**, L27 (2021).

[50] I. Legred, K. Chatziioannou, R. Essick, S. Han, and P. Landry, Impact of the PSR J0740+6620 radius constraint on the properties of high-density matter, Phys. Rev. D **104**, 063003 (2021).

[51] G. Raaijmakers *et al.*, Constraints on the dense matter equation of state and neutron star properties from NICER's mass–radius estimate of PSR J0740+6620 and multimessenger observations, Astrophys. J. Lett. **918**, L29 (2021).

[52] V. Doroshenko, V. Suleimanov, G. Pühlhofer, and A. Santangelo, A strangely light neutron star within a supernova remnant, Nat. Astron. **6**, 1444 (2022).

[53] J. E. Horvath, L. S. Rocha, L. M. de Sá, P. H. R. S. Moraes, L. G. Barão, M. G. B. de Avellar, A. Bernardo, and R. R. A. Bachega, A light strange star in the remnant HESS J1731−347: Minimal consistency checks, Astron. Astrophys. **672**, L11 (2023).

[54] Z. Miao, L. Qi, J. Zhang, A. Li, and M. Ge, Thermal x-ray studies of neutron stars and the equation of state, Phys. Rev. D **109**, 123005 (2024).

[55] P. Danielewicz, R. Lacey, and W. G. Lynch, Determination of the equation of state of dense matter, Science **298**, 1592 (2002).

[56] S. Typel and H. H. Wolter, Relativistic mean field calculations with density dependent meson nucleon coupling, Nucl. Phys. A **656**, 331 (1999).

[57] S. Typel, Relativistic model for nuclear matter and atomic nuclei with momentum-dependent self-energies, Phys. Rev. C **71**, 064301 (2005).

[58] K. A. Maslov, E. E. Kolomeitsev, and D. N. Voskresensky, Solution of the hyperon puzzle within a relativistic mean-field model, Phys. Lett. B **748**, 369 (2015).

[59] K. A. Maslov, E. E. Kolomeitsev, and D. N. Voskresensky, Relativistic mean-field models with scaled hadron masses and couplings: Hyperons and maximum neutron star mass, Nucl. Phys. A **950**, 64 (2016).

[60] E. E. Kolomeitsev, K. A. Maslov, and D. N. Voskresensky, Delta isobars in relativistic mean-field models with σ-scaled hadron masses and couplings, Nucl. Phys. A **961**, 106 (2017).

[61] K. A. Maslov, E. E. Kolomeitsev, and D. N. Voskresensky, Making a soft relativistic mean-field equation of state stiffer at high density, Phys. Rev. C **92**, 052801(R) (2015).

[62] W.-G. Paeng, H. K. Lee, M. Rho, and C. Sasaki, Interplay between ω-nucleon interaction and nucleon mass in dense baryonic matter, Phys. Rev. D **88**, 105019 (2013).

[63] M. F. M. Lutz, B. Friman, and C. Appel, Saturation from nuclear pion dynamics, Phys. Lett. B **474**, 7 (2000).

[64] A. S. Khvorostukhin, V. D. Toneev, and D. N. Voskresensky, Equation of state for hot and dense matter: σ–ω–ρ model with scaled hadron masses and couplings, Nucl. Phys. A **791**, 180 (2007).

[65] A. S. Khvorostukhin, V. D. Toneev, and D. N. Voskresensky, Relativistic mean-field model with scaled hadron masses and couplings, Nucl. Phys. A **813**, 313 (2008).

[66] A. S. Khvorostukhin, V. D. Toneev, and D. N. Voskresensky, Viscosity coefficients for hadron and quark-gluon phases, Nucl. Phys. A **845**, 106 (2010).

[67] E. E. Kolomeitsev, K. A. Maslov, and D. N. Voskresensky, Charged ρ-meson condensation in neutron stars, Nucl. Phys. A **970**, 291 (2018).

[68] K. A. Maslov and D. N. Voskresensky, RMF models with σ-scaled hadron masses and couplings for the description of heavy-ion collisions below 2 A GeV, Eur. Phys. J. A **55**, 100 (2019).

[69] K. Hebeler and A. Schwenk, Symmetry energy, neutron skin, and neutron star radius from chiral effective field theory interactions, Eur. Phys. J. A **50**, 11 (2014).

[70] S. Huth, C. Wellenhofer, and A. Schwenk, New equations of state constrained by nuclear physics, observations, and QCD calculations of high-density nuclear matter, Phys. Rev. C **103**, 025803 (2021).

[71] K. Maslov, N. Yasutake, D. Blaschke, A. Ayriyan, H. Grigorian, T. Maruyama, T. Tatsumi, and D. N. Voskresensky, Hybrid equation of state with pasta phases and third family of compact stars, Phys. Rev. C **100**, 025802 (2019).

[72] H. Grigorian, D. Blaschke, and D. N. Voskresensky, Cooling of neutron stars with color superconducting quark cores, Phys. Rev. C **71**, 045801 (2005).

[73] G. Baym, C. Pethick, and P. Sutherland, The ground state of matter at high densities: Equation of state and stellar models, Astrophys. J. **170**, 299 (1971).

[74] P. Haensel and A. Y. Potekhin, Analytical representations of unified equations of state of neutron-star matter, Astron. Astrophys. **428**, 191 (2004).

[75] L. Suleiman, M. Fortin, J. L. Zdunik, and P. Haensel, Influence of the crust on the neutron star macrophysical quantities and universal relations, Phys. Rev. C **104**, 015801 (2021).

[76] L. Suleiman, M. Fortin, J. L. Zdunik, and C. Providência, Polytropic fits of modern and unified equations of state, Phys. Rev. C **106**, 035805 (2022).

[77] J. L. Zdunik, M. Fortin, and P. Haensel, Neutron star properties and the equation of state for the core, Astron. Astrophys. **599**, A119 (2017).

[78] K. Masuda, T. Hatsuda, and T. Takatsuka, Hadron–quark crossover and massive hybrid stars with strangeness, Astrophys. J. **764**, 12 (2013).
[79] G. Baym, Confinement of quarks in nuclear matter, Physica A **96**, 131 (1979).
[80] T. Çelik, F. Karsch, and H. Satz, A percolation approach to strongly interacting matter, Phys. Lett. B **97**, 128 (1980).
[81] G. Baym, S. Furusawa, T. Hatsuda, T. Kojo, and H. Togashi, New neutron star equation of state with quark-hadron crossover, Astrophys. J. **885**, 42 (2019).
[82] T. Kojo, G. Baym, and T. Hatsuda, Implications of NICER for neutron star matter: The QHC21 equation of state, Astrophys. J. **934**, 46 (2022).
[83] S. Han and M. Prakash, On the minimum radius of very massive neutron stars, Astrophys. J. **899**, 164 (2020).
[84] D. D. Ofengeim, P. S. Shternin, and T. Piran, Maximal mass neutron star as a key to superdense matter physics, Astron. Lett. **49**, 567 (2023).
[85] S. Typel, M. Oertel, and T. Klähn, CompOSE compstar online supernova equations of state harmonising the concert of nuclear physics and astrophysics compose.obspm.fr, Phys. Part. Nuclei **46**, 633 (2015).
[86] J. S. Read, B. D. Lackey, B. J. Owen, and J. L. Friedman, Constraints on a phenomenologically parametrized neutron-star equation of state, Phys. Rev. D **79**, 124032 (2009).
[87] F. Özel and P. Freire, Masses, radii, and the equation of state of neutron stars, Annu. Rev. Astron. Astrophys. **54**, 401 (2016).
[88] D. D. Ofengeim, Universal properties of maximum-mass neutron stars: A new tool to explore superdense matter, Phys. Rev. D **101**, 103029 (2020).
[89] J. R. Stone, P. Guichon, H. Matevosyan, and A. Thomas, Cold uniform matter and neutron stars in the quark–meson-coupling model, Nucl. Phys. A **792**, 341 (2007).
[90] S. Kubis, W. Wójcik, D. A. Castillo, and N. Zabari, Relativistic mean-field model for the ultracompact low-mass neutron star HESS J1731-347, Phys. Rev. C **108**, 045803 (2023).
[91] J. Hu, S. Bao, Y. Zhang, K. Nakazato, K. Sumiyoshi, and H. Shen, Effects of symmetry energy on the radius and tidal deformability of neutron stars in the relativistic mean-field model, Prog. Theor. Exp. Phys. **2020**, 043D01 (2020).
[92] M. Evans *et al.*, A horizon study for cosmic explorer: science, observatories, and community, arXiv:2109.09882.
[93] C. D. Capano, I. Tews, S. M. Brown, B. Margalit, S. De, S. Kumar, D. A. Brown, B. Krishnan, and S. Reddy, Stringent constraints on neutron-star radii from multimessenger observations and nuclear theory, Nat. Astron. **4**, 625 (2020).